PHYSICAL REVIEW B VOLUME 55, NUMBER 24 15 JUNE 1997-II

Monte Carlo simulations of ballistic-electron-emission-microscopy imaging and spectroscopy of buried mesoscopic structures

E. Y. Lee and V. Narayanamurti
Electrical and Computer Engineering Department, University of California, Santa Barbara, California 93106

D. L. Smith
Los Alamos National Laboratory, Los Alamos, New Mexico 87545

(Received 14 March 1997; revised manuscript received 16 April 1997)

Monte Carlo simulations of the transport of electrons injected into the Γ valley of GaAs are performed for ballistic-electron-emission-microscopy (BEEM) imaging and spatially resolved spectroscopy of model quantum dots and quantum wires buried beneath the Au-GaAs interface. To determine the spatial resolution and the energy resolution of BEEM for such buried mesoscopic structures, the current fluxes and the electron normal wave vector distributions are obtained as a function of the depth from the Au-GaAs interface. The BEEM current cross sections and the spatially resolved BEEM spectra on and off these structures are calculated in order to study their dependence on the depth and the scanning-tunneling microscope tip-to-sample bias.[S0163-1829(97)02624-1]

Ballistic-electron-emission microscopy (BEEM) is a scanning-tunneling microscopy (STM) based technique that has been used to measure metal-semiconductor interface properties, such as Schottky energy barriers and to study hot carrier transport in thin metal films.[1–4] BEEM can be employed in both spectroscopy and microscopy modes. In the spectroscopy mode, the energy resolution is typically about 30 meV. Nanometer spatial resolution at the metal-semiconductor interface has been achieved experimentally in many metal-semiconductor systems, including GaAs,[1] $CoSi_2$/Si,[5] Au/SiO_2/Si,[6] Au/Si,[7,8] and metal GaP.[9,10] The Bell-Kaiser theory[2] has been extensively used to interpret the results. There has been significant effort in modeling of BEEM transport in the metal overlayer.[11–14]

Recently, BEEM has been used to investigate the electronic properties of objects buried below the metal-semiconductor interface. Laterally uniform heterojunctions have been explored, and the energy band offsets and the transmission properties of double barrier resonant tunneling structures have been investigated.[15–18] In addition, localized buried objects have been studied. BEEM imaging and spatially resolved spectroscopy of $In_xGa_{1-x}As$/GaAs misfit dislocations buried 700 Å below a Au-GaAs interface has recently been reported,[19] and a BEEM study of InAs quantum dots buried ~70 Å below a Au-GaAs interface has been described.[20] However, the mechanism of contrast in the BEEM imaging of such localized buried objects has not been thoroughly investigated. Although it has been shown[1,5–10] that the BEEM spatial resolution can be as good as a few nm at the metal-semiconductor interface, the resolution for probing buried objects is unknown.

Here we report results of Monte Carlo simulations of BEEM imaging and spectroscopy of objects buried beneath the Au-GaAs interface in order to answer questions regarding the BEEM spatial and energy resolution for buried mesoscopic structures and about the mechanism of BEEM contrast from such structures. For the Monte Carlo simulations, the initial electron flux distribution[21] $f_z(\varepsilon,\cos\theta)$ at the GaAs side of the Au-GaAs interface is specified by a modified Bell-Kaiser model. In this model, the kinematic Bell-Kaiser model[2] is supplemented by an interface transmission probability given by the quantum mechanical reflection from a step barrier[10] and also by the nonparabolicity of the Γ valley.[18] The explicit form for the flux distribution is

$$f_z(\varepsilon,\cos\theta)=\left(\frac{2}{\pi}\right)^2\frac{e^{-\delta/\zeta}}{\hbar^4}e^{-2gl}\frac{\sqrt{2m^*}k_z^m}{\left(\frac{k_z^m}{m}+\frac{k_z^s}{m^*}\right)^2}\times\theta(\mathrm{eV}-\varepsilon_b-\varepsilon)\varepsilon^{3/2}\cos^2\theta,$$

where the energy dependent effective mass $m^*=m_0^*(1+\alpha\varepsilon)$, $m_0^*=0.067m$, the nonparabolicity parameter $\alpha=0.69\ \mathrm{eV}^{-1}$, ε is the kinetic energy of the electron in the Γ valley, m is the free electron mass, δ is the thickness of Au, ζ is the attenuation length in Au, g is the WKB factor for planar tunneling, l is the tip-to-sample separation, ε_b is the Schottky barrier height, θ is the angle from the interface normal, k_z^m is the normal component of the k vector in the metal, and k_z^s is the normal component of the k vector in the semiconductor. We used this distribution and the von Neuman acceptance-rejection method[22] to inject electrons into the GaAs.

The structure used for the simulation is shown in Fig. 1. It consists of a thin layer of Au on an undoped GaAs epilayer that forms a drift region. At 2000 Å below the Au-GaAs interface is a collection plane. This collection plane models a delta doped layer that is often used in BEEM experiments to control the electric field in the semiconductor sample.[17] In the Monte Carlo simulation, the trajectory of each injected electron is followed in the drift region until it either reaches the collection plane or the Au-GaAs interface. The electrons scatter from phonons and intervalley scattering in the drift region. Electrons striking the object to be imaged are backscattered with a probability distribution determined by the electrical properties of the object. Backscattered electrons reaching the metal-semiconductor interface to not contribute to the BEEM current whereas those reaching a collection plane in the structure do.

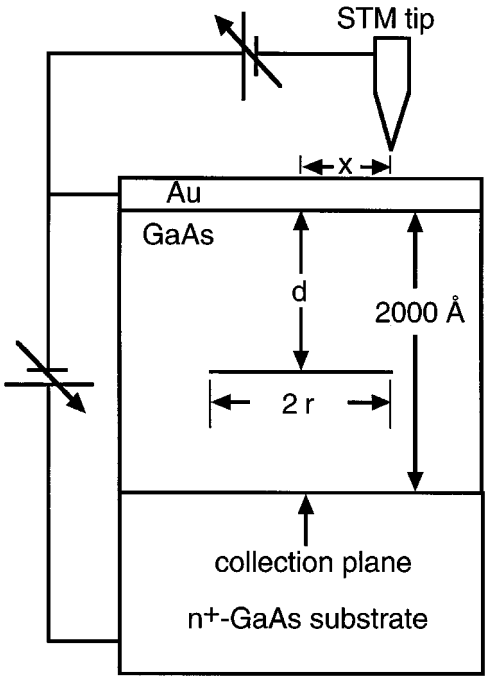

FIG. 1. Schematic of the structure used for the Monte Carlo simulations of BEEM imaging and spectroscopy. Not drawn to scale.

For the simulation of BEEM imaging and spatially resolved spectroscopy, the BEEM current is calculated as a function of the lateral displacement x between the STM tip, where the electrons are injected, and the center of the buried object, and as a function of the tip-to-sample bias V_t and the depth d of the object from the Au-GaAs interface. The tip-to-sample separation is taken to be 10 Å, a 1 nA constant tunneling current is assumed, and the spreading of the electron distribution in the Au overlayer is neglected. The electrons spread only a few nm within the Au,[1,5–10] which is insignificant in comparison to the spread in the GaAs. The temperature T and the electrical field E in the GaAs are adjustable, but they are fixed at $T=300$ K and $E=0$ kV/cm for the results reported here.

An overall intensity scaling factor is chosen to give approximately the experimentally observed BEEM current with no buried object present. When the tip-to-sample bias exceeds the Schottky barrier height of 0.92 eV, a fraction of the electrons injected into the Au can cross the Au-GaAs interface. For a tip-to-sample bias below 1.25 V, all the electrons are injected into the Γ valley of the GaAs because the next lowest conduction band valleys, the L valleys, are 0.33 eV above the Γ valley. Here, we only consider tip-to-sample bias of 1.25 V or below.

The transport of the electrons in the GaAs is simulated using Monte Carlo methods.[22–25] A three valley model is used to describe GaAs. Because the electrons are injected into the Γ valley and there is no field in the GaAs, the electrons largely stayed in the Γ valley. Details of the band structure and scattering parameters are taken from Refs. 23 and 25. Even when the BEEM current is calculated without a buried object, there is a reduction because of backscattering by phonons. The extent of this reduction depends on the position of the collection plane and the size of the electric field in the GaAs. For the parameters used here (the collection plane 2000 Å below the interface, zero electric field, and

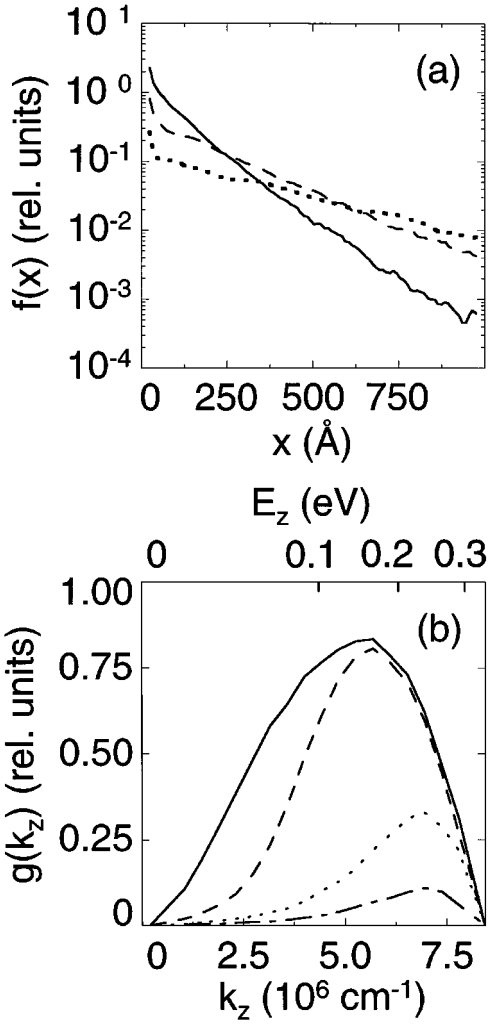

FIG. 2. (a) The normalized flux of BEEM electrons as a function of lateral displacement at 100 (solid line), 300 (dashed line), and 600 (dotted line) Å below the Au-GaAs interface. (b) The electron distribution with respect to k_z passing through a 300 Å disk centered laterally at the STM tip located at the Au-GaAs interface (solid line), 100 Å below (dashed line), 300 Å below (dotted line), and 600 Å below (dash-dotted line) the interface.

300 K), the reduction in the BEEM current by scattering varies between about 50% at the threshold bias to about 30% at the highest bias considered. These numbers decrease as the electric field is increased or the collection plane is moved closer to the interface.

The normalized electron flux $f(x)$ at a distance of $d=\{100,300,600\}$ Å below the Au-GaAs interface is calculated and it is shown in Fig. 2(a). The tip-to-sample bias V_t is 1.25 V. $f(x)$ broadens with increasing d and decays rapidly with increasing x. It is larger near $x=0$ and decreases more rapidly with increasing x for smaller values of d. Figure 2(b) shows the normal wave vector distribution $g(k_z)$ of electrons incident upon a 300 Å diameter disk at a lateral displacement of $x=0$ and depths of $d=\{0, 100, 300, 600\}$ Å below the Au-GaAs interface. $g(k_z)$ at $d=0$ Å is the injected distribution. The tip-to-sample bias is 1.25 V and E_z, the contribution to the energy from the normal wave vector component, is shown on the upper axis of Fig. 2(b). The distribution decrease in overall magnitude with increasing depth due to the spatial broadening of the electron flux. The normal wave vector distribution narrows for $d=100$ and

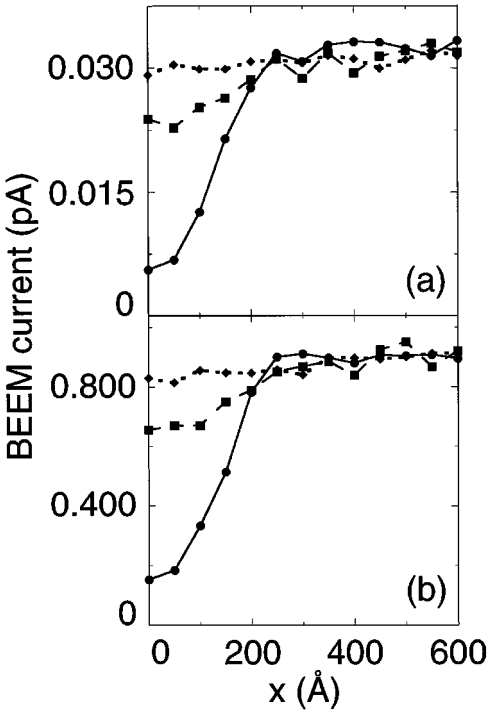

FIG. 3. The BEEM current as a function of lateral displacement at a tip-to-sample bias of 1 V (a) and 1.25 V (b) for a perfectly reflecting quantum dot 300 Å in diameter. The lines are drawn as a guide for the eye. In both (a) and (b), the solid line (circle) is for $d=100$ Å, the dashed line (square) is for $d=300$ Å, and the dotted line (diamond) is for $d=600$ Å.

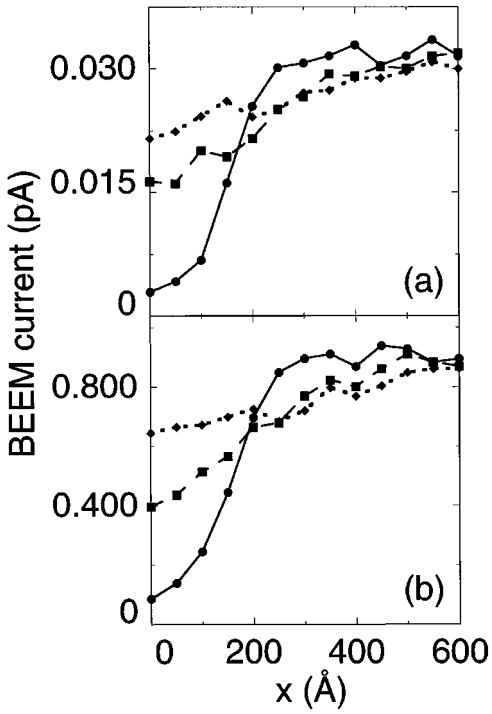

FIG. 4. The BEEM current as a function of lateral displacement at a tip-to-sample bias of 1 V (a) and (b) 1.25 V for a perfectly reflecting quantum dot 300 Å in diameter. The lines are drawn as a guide for the eye. In both (a) and (b), the solid line (circle) is for $d=100$ Å, the dashed line (square) is for $d=300$ Å, and the dotted line (diamond) is for $d=600$ Å.

300 Å, because only those electrons with k_x and k_y small with respect to k_z hit the disk away from the interface. However, at 600 Å, $g(k_z)$ starts to widen again due to electrons that underwent scattering before hitting the target. The sharpest k_z and energy distribution incident upon the ''target'' occurs at a depth between 300 and 600 Å.

We consider the depth and the voltage dependence of the BEEM current for a buried quantum dot (QD). The QD is modeled by a thin disk 300 Å in diameter, which specularly scatters electrons of all energies. Later, we consider a more realistic transmission behavior for a specific case, but we treat this idealized case here, to obtain general results. Because the QD is relatively thin, the scattering from its edge is neglected. This is a model for a self assembled quantum dot[26] with a large conduction band offset, such as an AlSb dot grown on GaAs. Figure 3 shows the calculated BEEM current as a function of the lateral distance for (a) tip bias voltage $V_t=1.00$ V and (b) $V_t=1.25$ V. For each point, 1000 electrons are used for the simulation. The BEEM current has a dip when the STM tip is over the QD and it gradually increases to approach an asymptotic value as x increases. The dip in the BEEM current occurs because electrons are backscattered by the QD and return to the Au-GaAs interface without contributing to the BEEM current. If the QD is placed deeper away from the interface, the contrast in the BEEM current decreases due to the spread of the electron distribution with depth. There is very little contrast for a depth of 600 Å. Even though there is a large difference in the overall magnitude of the BEEM current, the shape of the BEEM contrast does not change significantly with tip-to-sample bias between 1.00 and 1.25 V. This reflects the nearly constant total scattering rate of the Γ electrons in this energy range, due to a simultaneous decrease of the polar optical phonon scattering rate and increase of the acoustic phonon scattering rate with energy.[25]

The injected electrons have approximately a $\cos^2\theta\, d(\cos\theta)$ angular distribution and if they traveled ballistically in the GaAs, the fraction of electrons that would not be backscattered from the QD at $x=0$ would be $[1+(r/d)^2]^{-3/2}$, where d is the depth of the QD and r is its radius. The mean-free path for scattering is about 500 Å for the electron energy range considered here. For values of d much less the 500 Å the ballistic expression describe the magnitude of the dip in the Monte Carlo simulations reasonably well. For larger values of d, electron scattering degrades the spatial resolution faster than expected from a ballistic model.

As a model for a quantum wire (QW) with a large conduction band offset, we consider a thin 300 Å wide stripe that specularly reflects electrons of all energies. Figure 4 shows the calculated BEEM current as a function of lateral distance for (a) $V_t=1.00$ V and (b) $V_t=1.25$ V. For each point, 1000 electrons are used for the simulation. Qualitatively, the voltage and the spatial dependencies are similar to that of a QD. However, being a one-dimensional (1D) object rather than a zero-dimension object like a QD, the BEEM contrast is in general stronger for a QW. In comparing Figs. 3 and 4, it can be seen that the dips are deeper in Fig. 4. The BEEM contrast decreases more slowly with the depth of the object. At a depth of 600 Å, a QD is hardly detectable by BEEM whereas the QW still shows significant contrast.

In Fig. 5 we compare the calculated BEEM spectrum taken directly on a large energy offset QD that scatters all incident electrons specularly to the spectrum on a 30-Å-thick QD has an energy offset of 0.15 eV. The transmission prob-

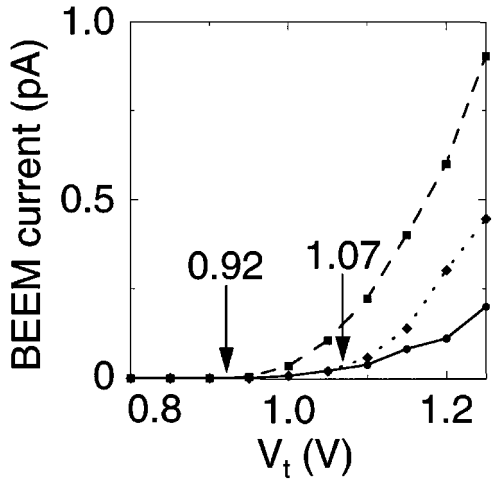

FIG. 5. The calculated BEEM current as a function of tip-to-sample bias when the STM tip is directly over (circle and solid line) and far from (square and dashed line) a perfectly reflecting quantum dot 300 Å in diameter placed 100 Å below the Au-GaAs interface. Also shown is the spectrum for a 300 Å wide and 30 Å quantum dot that has transmission probability determined by the standard quantum mechanical 1D transmission function for a finite barrier 0.15 eV tall. The Au-GaAs Schottky barrier height of 0.92 eV and the energy barrier of the QD (0.92+0.15 eV) are indicated by arrows.

ability through the second QD is calculated using the quantum mechanical 1D transmission function for a finite barrier. A spectrum with no buried object near the STM tip is also shown. For each point, 1000 electrons are used for the simulation. The QD's are both 100 Å below the interface and have a 300 Å diameter. All the spectra have an initial turn on at 0.92 eV, the Au-GaAs Schottky barrier height. Compared to the off-QD case, the BEEM current is suppressed by an almost bias independent factor by the large barrier QD. Comparing the low barrier QD spectrum to the high barrier one, we see that the two spectra are the same for low bias. However, when the bias exceeds the barrier height of the QD at 1.07 V, the BEEM current on the low barrier QD increases more rapidly. By comparing such simulated BEEM spectra to experimental data, it should be possible to determine the local barrier heights of buried objects.

In summary, we have performed Monte Carlo simulations of electron transport in GaAs for BEEM imaging and spatially resolved spectroscopy of model quantum dots and quantum wires. For spatial and energy resolution of BEEM, the current fluxes and the electron normal vector distributions are obtained as a function of the depth. Decrease of the BEEM spatial resolution with the depth is seen, and a range of optimum depths for the sharpest crystal momentum and energy distribution of the electrons incident upon the buried structure is found, due to an interplay between a geometric filtering effect and the role of the electron-phonon scattering. Simulation of BEEM imaging is carried out. For a quantum wire, significantly more BEEM contrast than a quantum dot is seen, due to added dimensionality. Simulations of spatially resolved spectroscopy on and off model quantum dots are performed. By comparing Monte Carlo simulations to experiments, it should be possible to deduce the local electronic properties of buried mesoscopic structures. Future work will address higher tip-to-sample bias regimes, the dependence on the temperature, the dependence on the electric field in the GaAs, and alternative models of quantum dots and wires.

The authors gratefully acknowledge partial funding from AFOSR (Grant No. 442530-22502). The work of D. L. S. is conducted under the auspices of the Department of Energy, supported in part by funds provided by the University of California for the conduct of discretionary research by Los Alamos National Laboratory.

[1] W. J. Kaiser and L. D. Bell, Phys. Rev. Lett. **60**, 1406 (1988).
[2] L. D. Bell and W. J. Kaiser, Phys. Rev. Lett. **61**, 2368 (1988).
[3] M. Prietsch, Phys. Rep. **253** 163 (1995).
[4] L. D. Bell and W. J. Kaiser, Annu. Rev. Mater. Sci. **26** 189 (1996).
[5] H. Sirringhaus, E. Y. Lee, and H. von Känel, Phys. Rev. Lett. **73**, 577 (1994).
[6] A. M. Milliken, S. J. Manion, W. J. Kaiser, L. D. Bell, and M. H. Hecht, Phys. Rev. B **46**, 12 826 (1992).
[7] H. D. Hallen, A. Fernandez, T. Huang, J. Silcox, and R. A. Burhman, Phys. Rev. Lett. **69**, 2931 (1992).
[8] H. A. Palm and M. Schulz, Phys. Rev. Lett. **71**, 2224 (1993).
[9] R. Ludeke, M. Prietsch, and A. Samsavar, J. Vac. Sci. Technol. B **9**, 2342 (1991).
[10] M. Prietsch and R. Ludeke, Phys. Rev. Lett. **66**, 2511 (1991).
[11] L. J. Schowalter and E. Y. Lee, Phys. Rev. B **43**, 9308 (1991).
[12] A. Bauer, M. T. Cuberes, M. Prietsch, and G. Kaindl, Phys. Rev. Lett. **71**, 149 (1993).
[13] Mao-long Ke, D. I. Westwood, C. C. Matthai, B. E. Richardson, and R. H. Williams, Phys. Rev. B **53**, 4845 (1996).
[14] F. J. Garcia-Vidal, P. L. de Andres, and F. Flores, Phys. Rev. Lett. **76**, 807 (1996).
[15] J. J. O'Shea, C. M. Reaves, S. P. DenBaars, M. A. Chin, and V. Narayanamurti, Appl. Phys. Lett. **69**, 3022 (1996).
[16] S. Bhargava, H.-R. Blank, V. Narayanamurti, and H. Kroemer, Appl. Phys. Lett. **70**, 759 (1997).
[17] T. Sajoto, J. J. O'Shea, S. Bhargava, D. Leonard, M. A. Chin, and V. Narayanamuriti, Phys. Rev. Lett. **74**, 3427 (1995).
[18] D. L. Smith and Sh. M. Kogan, Phys. Rev. B **54**, 10 354 (1996).
[19] E. Y. Lee, S. Bhargava, K. J. Pond, K. Luo, M. A. Chin, and V. Narayanamurti, Appl. Phys. Lett. **69**, 940 (1996).
[20] M. E. Rubin, G. Medeiros-Ribeiro, J. J. O'Shea, M. A. Chin, E. Y. Lee, P. Petroff, and V. Narayanamurti, Phys. Rev. Lett. **77**, 5268 (1996).
[21] The BEEM current equals the integral of the flux distribution $f_z(\varepsilon,\cos\theta)$ over ε and $\cos\theta$ multiplied by the electron charge and the tunneling area.
[22] C. Jacobini and L. Reggiani, Rev. Mod. Phys. **55**, 645 (1983).
[23] K. Brennan and K. Hess, Solid State Electron. **27**, 347 (1984).
[24] W. Fawcett, A. D. Boardman, and S. Swain, J. Phys. Chem. Solids **31**, 1963 (1970).
[25] G. M. Wysin, D. L. Smith, and Antonio Redondo, Phys. Rev. B **38**, 12 514 (1988).
[26] Self-assembled quantum dots are typically about 200–300 Å in diameter, as seen by TEM, and about 30 Å high, as measured by AFM; see, for example, D. Leonard, M. Krishnamurthy, C. M. Reaves, S. P. DenBaars, and P. M. Petroff, Appl. Phys. Lett. **63**, 3203 (1993).